VAMP2 and synaptotagmin mobility in chromaffin granule membranes: implications for regulated exocytosis

Prabhodh S. Abbineni[a,b,*], Joseph S. Briguglio[c], Edwin R. Chapman[c], Ronald W. Holz[b], and Daniel Axelrod[b,d]

[a]Life Sciences Institute and Departments of [b]Pharmacology and [d]Physics, University of Michigan, Ann Arbor, MI; [c]Howard Hughes Medical Institute, Department of Neuroscience, University of Wisconsin, Madison, WI

ABSTRACT **Granule-plasma membrane docking and fusion can only occur when proteins that enable these reactions are present at the granule-plasma membrane contact. Thus, the mobility of granule membrane proteins may influence docking and membrane fusion. We measured the mobility of vesicle associated membrane protein 2 (VAMP2), synaptotagmin 1 (Syt1), and synaptotagmin 7 (Syt7) in chromaffin granule membranes in living chromaffin cells. We used a method that is not limited by standard optical resolution. A bright flash of strongly decaying evanescent field produced by total internal reflection was used to photobleach GFP-labeled proteins in the granule membrane. Fluorescence recovery occurs as unbleached protein in the granule membrane distal from the glass interface diffuses into the more bleached proximal regions, enabling the measurement of diffusion coefficients. We found that VAMP2-EGFP and Syt7-EGFP are mobile with a diffusion coefficient of ~3 × 10^{-10} cm^2/s. Syt1-EGFP mobility was below the detection limit. Utilizing these diffusion parameters, we estimated the time required for these proteins to arrive at docking and nascent fusion sites to be many tens of milliseconds. Our analyses raise the possibility that the diffusion characteristics of VAMP2 and Syt proteins could be a factor that influences the rate of exocytosis.**

Monitoring Editor
Diane Lidke
University of New Mexico

Received: Oct 18, 2021
Revised: Nov 10, 2021
Accepted: Nov 23, 2021

INTRODUCTION

Enormous progress has been made in understanding the protein interactions and events leading to fusion of secretory granules and synaptic vesicles with the plasma membrane. Nevertheless, the final events leading to fusion remain uncertain. Granules must move into intimate contact with the plasma membrane in order for granule membrane and plasma membrane proteins to interact to initiate the fusion reaction. These proteins include the granule SNARE protein VAMP2 (synaptobrevin-2) and the Ca^{2+} sensor synaptotagmin and the plasma membrane acceptor complex composed of the t-SNARES, SNAP25 and syntaxin (Jahn and Fasshauer, 2012; Rizo and Südhof, 2012). It has not been established when these interactions occur. On the one hand, the initial interactions may create a stable intermediate that participates in the docking of secretory granules, and awaits a Ca^{2+} signal to pull the membranes together to initiate fusion (Nofal *et al.*, 2007; Karatekin *et al.*, 2008; Sudhof, 2013). Alternatively, the constantly jittering granules (Allersma *et al.*, 2006; Degtyar *et al.*, 2007) only interact with the plasma membrane milliseconds or less before fusion. Indeed, it has been suggested that the strongly energy-favorable interactions of opposing SNARE proteins may not allow a stable intermediate (Jahn and Fasshauer, 2012); once engaged, the interactions proceed rapidly to fusion.

Close approximation of the granule and plasma membrane does not guarantee productive protein interactions. A kinetic factor in fusion that has not been considered is the speed with which proteins access the ultimate fusion site. Although the dynamics of syntaxin and SNAP25 in the plasma membrane have been studied (Barg *et al.*, 2010; Knowles *et al.*, 2010; Gandasi and Barg, 2014; Yin *et al.*, 2018)

This article was published online ahead of print in MBoC in Press (http://www.molbiolcell.org/cgi/doi/10.1091/mbc.E21-10-0494) on December 1, 2021.

The authors declare no competing interests.

Data sharing plan: All data, reagents, and software programs used in the manuscript will be shared upon request.

*Address correspondence to: Prabhodh Abbineni (pabbinen@umich.edu).

Abbreviations used: EPI, epifluorescence; IDL, interactive data language; PSS, physiological salt solution; Syt1, synaptotagmin 1; Syt7, synaptotagmin 7; TIR-FRAP, TIR-fluorescence recovery after photobleaching; TIR, total internal reflection; VAMP2, vesicle associated membrane protein 2.

little is known about the state of VAMP2 and Syt in the secretory granule membrane. Their mobility and distribution in the granule membrane likely influence the pathway to fusion. For example, if VAMP2 and synaptotagmin are immobile, nanometer distance apposition of the two membranes would result in fusion only if, by chance, the cognate proteins are already present and properly oriented to enable interaction. On the other hand, if the secretory granule proteins are mobile, diffusion could facilitate interaction.

In this study we have investigated the mobility of VAMP-2, synaptotagmin1 (Syt1), and synaptotagmin7 (Syt7) in the secretory (chromaffin) granule membrane in living chromaffin cells. We adapted a method that is not limited by standard optical resolution that we had previously developed to measure the mobility of granule lumenal proteins (Weiss *et al.*, 2014). Granules are bleached in a strongly decaying evanescent field (~80 nm exponential decay constant) produced by total internal reflection (TIR). Because the diameter of bovine chromaffin granules is ~300 nm (Plattner *et al.*, 1997), the high-intensity excitation selectively bleaches fluorophore-label protein proximal to the glass interface in the membrane of individual chromaffin granules. Fluorescence recovery can occur as unbleached protein from the more distal surface of the granule diffuses into the proximal bleached regions. This experimental approach, a variation of TIR-fluorescence recovery after photobleaching (TIR-FRAP; Thompson *et al.*, 1981) introduced for open areas in 1981, is accompanied by a new theoretical and quantitative analysis that takes into account the limited number of total fluorophore molecules on the granule membrane, diffusion in the spherical membrane, granule diameter, the evanescent field depth, and the duration of the bleach. In the course of the experiments, we discovered additional experimental factors that had to be considered: light scattering that accompanies TIRF excitation, and reversible bleaching of the GFP-based fluorophores and its relationship to irreversible bleaching. Finally, we consider the influence of VAMP2 and Syt diffusion on initiating fusion and subsequent fusion pore expansion.

THEORY

In these experiments, a secretory granule (modeled as a 300-nm-diameter hollow sphere) is embedded in an evanescent field (created by TIR) with an exponentially decaying characteristic depth (80 nm). There are two possible versions of the experiment. One version is for fluorophore-labeled membrane proteins confined to two-dimensional diffusion on the granule surface (the focus of the current study). The other version is for fluorophore-labeled lumenal proteins confined to three-dimensional diffusion within the granule interior (described previously; Weiss *et al.*, 2014). The qualitative interpretations and relevant complications for the two versions of experiments are the same; the only difference lies in the quantitative theoretical interpretation.

The experimental protocol for the two versions is the same. A dim "probe" intensity of the evanescent field excites fluorescence, predominantly but not exclusively, near the "bottom" of the sphere where the sphere is proximal to the TIR substrate (the coverslip) and the evanescent field is strongest. The total TIR-excited fluorescence from the whole sphere is measured and normalized to unity. Then, the illumination intensity is increased in a single step to a factor of ~100 higher for a duration of 46 ms (for membrane proteins) or 169 ms (for lumenal proteins), which leads to significant bleaching of the fluorophore, especially but not exclusively at the granule bottom. Then after the bleach, the evanescent intensity is reduced to its prebleach level, and the emitted total fluorescence intensity is tracked versus time, as unbleached fluorophores diffuse around (or in) the sphere toward a uniform distribution.

In principle, the form of the recovery could be calculated (perhaps numerically) from an explicit differential equation. However, there are several significant real-world factors that make the solution, and the ultimate determination of the diffusion coefficient, somewhat more complicated:

1. The excitation itself is not a pure TIR-produced exponential decay, but contains some fraction of its intensity arising from scattering, originating either from the microscope optics (Brunstein *et al.*, 2014a,b) or from refractive index irregularities in the sample itself (Axelrod and Axelrod, 2021). That scattering fraction can lead to its own bleaching during all phases of the experiment. The actual excitation intensity thereby is a sum of the exponentially decaying evanescent part plus a z-independent scattering part, estimated here to be an additional ~20% of the $z = 0$ evanescent intensity.
2. The timescale of the experiments is short, on the order of tens to hundreds of milliseconds. On that timescale, bleaching is not entirely irreversible; some bleached fluorophores return spontaneously to a ground state (e.g., a return from a long-lived triplet state), capable of reexcitation to a fluorescence-producing excited state. This reversible recovery must be distinguished from the diffusion-based recovery.
3. The mechanism of reversible bleaching and its relationship to irreversible bleaching are not well known. Possible modes include the following. A) Reversible and irreversible bleaching are parallel processes occurring only to an unbleached fluorophore, each type of bleaching with its own fixed likelihood proportional to the illumination intensity. B) Irreversible bleaching can only occur to a fluorophore that is already in a "reversibly bleached state" but which has not yet returned to the ground state. The irreversibly bleached outcome is a random event entirely independent of illumination intensity. C) Irreversible bleaching can occur only to a fluorophore that is already in a reversibly bleached state, but irreversible bleaching requires another photon to be absorbed, beyond that which created the reversibly bleached state. Each of these possibilities would lead to a different dependence of ratio of reversible:irreversible bleach depth as the incident illumination intensity is changed, and a different amount of bleaching that occurs during the probe phase of the experiment (see below). The question of which mode is correct can be investigated by examining reversible versus irreversible bleach depth under epifluorescence (EPI) illumination. (In EPI, the excitation intensity through the entire depth of the granule is constant, and diffusion-related effects would thereby become irrelevant.) Our observations are most consistent with mode C. Reversible bleaching is a complication, but its presence actually makes fast TIR/FRAP experiments possible. There would not be enough bleaching during very short bleaching pulses if it were not for reversible (and quickly recovering) reversible bleaching. If experiments had been at a much longer timescale, reversible bleaching would not be evident, but that would be too long to see the diffusion effects that motivate the experiments.
4. During the prebleach and postbleach dim "probe" phase, significant bleaching (either reversible or irreversible or both) can occur, which tends to cause a loss of fluorescence. Because the illumination is z dependent, even probe phase bleaching occurs nonuniformly around the sphere's surface or in its interior.
5. During the finite-time duration of the bright "bleach" phase, significant diffusion of the fluorophore can occur, making the $t = 0$ distribution of fluorophores immediately at the end of the bleach phase somewhat poorly defined.

6. Each granule may be located at a slightly different distance from the TIR/coverslip surface and thereby sees a different evanescent illumination intensity. This variability will manifest as a different $t = 0$ postbleach fluorescence. That variability will affect the postbleach distribution of unbleached fluorophores and ultimately the exact form and timescale of the fluorescent recovery. For this reason, results are grouped and averaged into several separate ranges of bleach depth.

To account for all these complications, we use a custom Monte Carlo–type program (written in interactive data language [IDL] and named "diffusionshellsim") that repeatedly simulates the diffusion as a virtual random walk of a single fluorophore molecule. A simulated membrane protein diffusing on a spherical surface, or within the sphere, is first positioned at a random location in its realm. During its walk, the fluorescence versus time it produces is calculated and recorded from its z position (the distance from the TIR/coverslip surface), given a z-dependent excitation illumination intensity that includes both evanescent decay and scattering. That molecule is tracked over its entire random walk course versus time until it irreversibly bleaches. Then another molecule is launched from a new random location. Altogether, a complete simulation consists of summing the fluorescence versus time of tens of thousands of such single molecule tracks.

Here is more detail on this procedure, and how the complications are handled. Time is divided into a large (consistent with an acceptable total computation time) but finite number of time increments (each with a duration of 1 ms), out to a simulated time of some $t = t_{max}$. For surface-confined membrane proteins, in each time increment in sequence, two new normally distributed random numbers (symmetrical around zero) are generated: one to compute the random length (generally $\ll R$) of a single step to a new location and the other its random direction angle from its starting point on the surface. After appropriate geometrical considerations involving rotation matrices, the z position of the new location is calculated. The average of the length squared of the diffusive step vectors is scaled to be proportional to an input parameter diffusion coefficient D.

For volume-confined lumenal proteins, we use a related custom IDL program named diffusionspheresim. In each time increment in sequence, three new normally distributed random numbers (symmetrical around zero) are generated, one for each of the three orthogonal dimensions, with the average step size corresponding to a user-specified diffusion coefficient. If the next step places the molecule outside the sphere by some distance l from the surface, it is "reflected" back into the sphere to a location along the same radial line and the same distance from the surface.

All of the above effects 1)–6) can be incorporated into each incremental step by using additional input parameters. These parameters, and how they are determined, are explained as follows:

1. *The characteristic rate (in s^{-1}) for reversible bleach recovery.* This rate parameter can be determined directly from experimental data taken on granules with EPI illumination (i.e., subcritical angle) instead of TIR illumination optics using the same bleach-and-probe intensity variation protocol. Because EPI illumination is not z dependent at the sample, the time dependence of the consequent fluorescence recovery, if any, is entirely due to reversible recovery.
2. *A "total bleaching" parameter, proportional to local excitation intensity, that determines the immediately postbleach ($t = 0$) fluorescence.* This parameter can be varied in the simulation program to produce simulated fluorescence at $t = 0$ that matches that of the average of a group of similar-bleach-depth experimental runs.
3. *The ratio of probe-to-bleach illumination, which is known by direct premeasurements of laser intensity entering the microscope.*
4. *The ratio of the reversible to irreversible bleaching probabilities.* This parameter strongly affects the ratio of the fluorescence at $t = 0$ to the long-time "plateau" fluorescence (measured in practice at $t = t_{max}$) in the EPI illumination experiments (which are insensitive to diffusion). This ratio can be adjusted in the simulation, essentially by trial and error, to produce simulated EPI results that correspond to the experimentally observed EPI fluorescence ratio for $t = 0$ to $t = t_{max}$.
5. For reversible bleaching mode B, we adjust a light-independent rate input parameter at which a spontaneous conversion from the reversible to irreversible bleached state occurs. For mode C, we adjust an input parameter that relates the efficiency of absorption of the first photon (which leads to reversible bleaching) to the efficiency of absorption of the second photon (which leads to irreversible bleaching from the reversibly bleached state).
6. Light scattering is introduced as a z-independent term in the incident light intensity with its amplitude (relative to the evanescent decaying part) characterized by an input parameter.

These input parameters can be converted to single step probabilities that a molecule will be either left unbleached, reversibly bleached, recovered from prior reversible bleaching, or irreversibly bleached. Any probability (say, p) is realized in the simulation by uniformly randomly generating a number between 0 and 1 and proceeding appropriately if the number turns out to be less than p. If the molecule does not get irreversibly bleached, it "survives" to make the next diffusive step on the sphere, and the process of determining its fluorescence and its bleach status is repeated. If the molecule is irreversibly bleached at any step, its fluorescence versus time history up to that time is added to that of previous molecule fluorescence histories, and then a new molecule is started at a random position. After a preset number of molecules (usually in the tens of thousands) is reached, the final accumulated fluorescence versus time curve is the simulation program's output.

The overall goal is to determine the one remaining parameter, the diffusion coefficient D. Simulations with the correct bleaching parameters are run for a range of possible D values. The simulated results are then compared with the corresponding experimental TIR data (the average of runs with similar bleaching depths) by calculating the average unweighted chi-square difference between the experimental and the simulated curve. The D for which the chi-square value is at a minimum is deemed to be the correct diffusion coefficient.

RESULTS

Simulation of diffusion on the surface of a sphere

Following photobleaching with TIR excitation, a gradient of fluorescence is imprinted on the granule membrane (Figure 1A), as the evanescent field decay constant (~80 nm) is shorter than the diameter of chromaffin granules (~300 nm). Redistribution of fluorophores into the bleached region by diffusion leads to at least partial dissipation of the gradient (Figure 1A; compare immobile and mobile fluorophores). The faster the diffusion, the more rapidly the gradient suffers dissipation.

We utilized two related methods that rely on photobleaching with TIR excitation to measure the diffusion of fluorophore-tagged

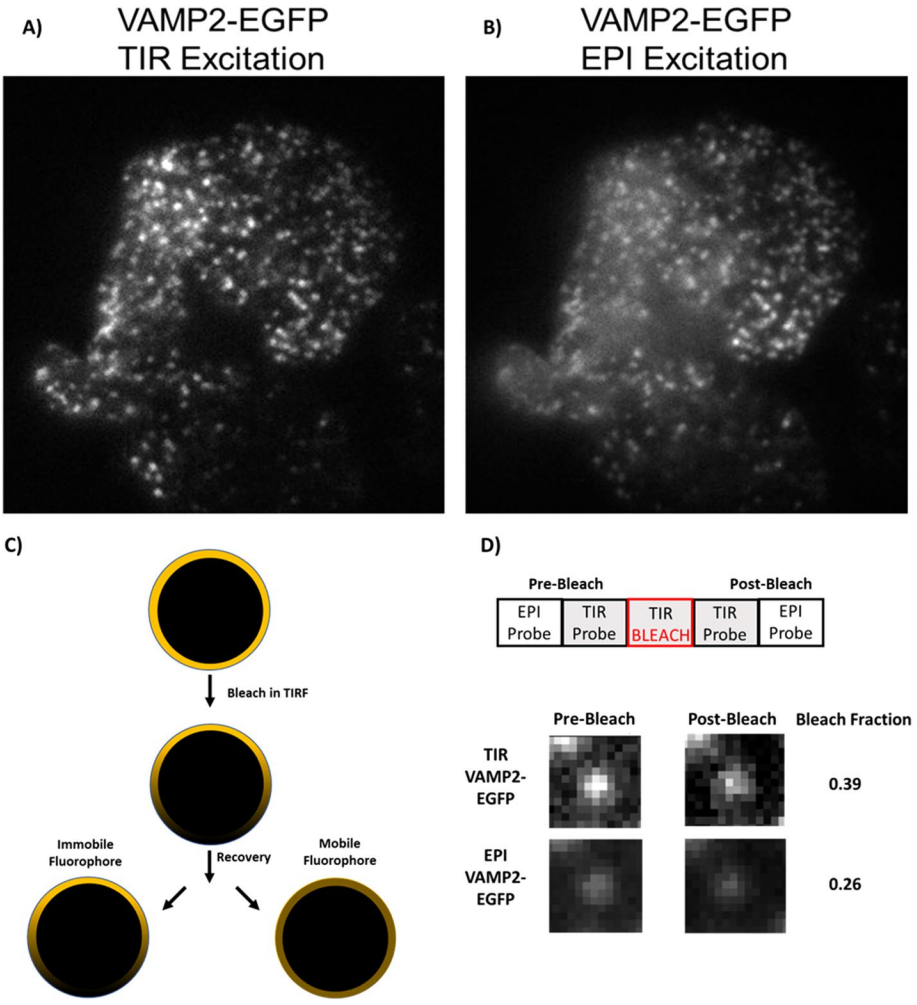

FIGURE 1: TIR-based photobleaching protocol to measure the mobility of chromaffin granule membrane proteins. Image of a chromaffin cell expressing VAMP2-EGFP imaged using low-intensity TIR (A) or EPI (B) illumination. (C) Schematic of the principle underlying the TIR-FRAP method. Chromaffin granules labeled with a fluorophore-tagged membrane protein are photobleached using TIR excitation light. The gradient of bleached fluorophore imprinted on the granule membrane dissipates over time if the protein is mobile, or remains stable if the protein is immobile. (D) Fluorescence of the granules is measured using low-intensity TIR and EPI illumination before and after bleaching in TIR. Shown is an example of a typical granule labeled with VAMP2-EGFP. The bleach depth (fraction of fluorescence lost) in TIR and EPI is calculated, 1-F(postbleach)/F(prebleach).

VAMP2, Syt1, and Syt7 on chromaffin granule membranes. a) The first method ("bleach depth") measures the presence of the gradient by measuring the fluorescence intensity of the granules before and after a TIR bleach using two kinds of probe illumination in rapid sequence: first, a low-intensity TIR evanescent field that excites the region that will be subsequently bleached or just has been bleached; and second, an EPI illumination probe that excites uniformly the whole granule. If a gradient of fluorescence has been imprinted, the bleach depth (fraction of fluorescence lost) measured by TIR is greater compared with the bleach depth measured by EPI, as TIR selectively probes the TIR-photobleached region. b) The second method ("FRAP") involves monitoring fluorescence recovery over time following photobleaching with TIR excitation. As TIR selectively photobleaches fluorophores proximal to the glass interface, fluorescence recovery occurs as distal fluorophores diffuse into the bleached area.

We derive by simulation the expected results for highly mobile and relatively immobile fluorophores, and then consider the influence of scattered light, which contaminates the evanescent field, on the expected results.

The influence of scattering on TIR/EPI bleach depth measurements

For highly mobile proteins, the bleach depth (i.e., the fraction of fluorescence lost) is identical when measured by TIR or EPI illumination (Figure 2A, solid 45° line), as the rapidly diffusing proteins uniformly distribute on the surface of the granule during the photobleaching step. For slowly diffusing proteins, the bleach depth as measured by TIR is relatively higher compared with the bleach depth measured by EPI illumination (Figure 2A, dotted line), as TIR selectively probes the photobleached region. However, in experimental settings, the evanescent field is not pure and is contaminated by scattered light originating either from the microscope optics (Brunstein *et al.*, 2014a,b) or from refractive index irregularities in the cell (Axelrod and Axelrod, 2021). Previous measurements using a 1.65 numerical aperture (NA) lens and fluorescent beads estimated that ~10% of the evanescent field is contaminated by scattered light at the coverslip/sample interface (Mattheyses and Axelrod, 2006). Given the heterogeneous refractive index of the cell imaged in the evanescent field (Axelrod and Axelrod, 2021), we expect the degree of scattering to be greater than 10%. Thus, we derived the expected result for TIR/EPI bleach depth for fluorophores on a surface of a hypothetical sphere in evanescent field containing 0, 10%, or 20% scattered light at the coverslip/sample interface (Figure 2A) containing 0, 10%, or 20% scattered light at the coverslip/sample interface (Figure 2A, dotted and dashed lines). For Figure 2A, we assumed a D of 3×10^{-10} cm^2/s; this value of D is within the range predicted by the recovery data (see below). As scattered light is not spatially selective, it photobleaches fluorophores uniformly on the surface of the granules, and decreases the difference between the bleach depths measured by low-intensity TIR and EPI illumination and influences the sensitivity of our measurements. We then simulated the diffusion of fluorophores with varying D with 20% scattering present in the evanescent field (Figure 2B). Scattering reduced but did not eliminate the difference between TIR and EPI bleach depths.

The influence of scattering on TIR-FRAP measurements

Similar to the TIR/EPI bleach depth simulations described above, we simulated time-dependent fluorescence recovery following TIR photobleaching and either varied the degree of scattering (0, 10%, or 20%) present in the evanescent field while considering a single D of 3×10^{-10} cm^2/s (Figure 2C), or varied D while including 20%

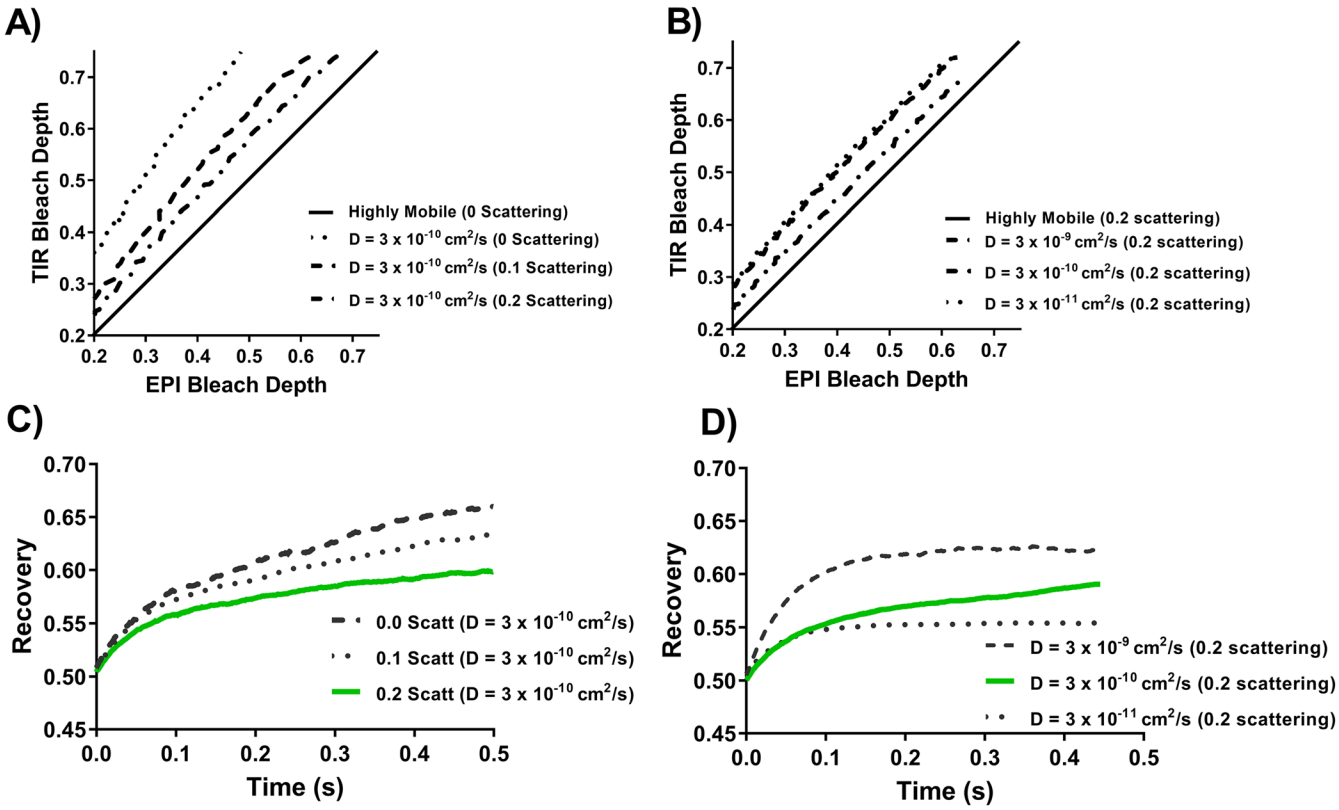

FIGURE 2: Simulation of diffusion on the surface of a sphere. Fluorescent proteins with a given diffusion coefficient (D), present on the surface of a 300-nm sphere, were photobleached for 45 ms in an evanescent field with a decay constant of 80 nm. The bleach depth (fraction of fluorescence lost) evident by TIR and EPI illumination (A, B), and fluorescence recovery following photobleaching (C, D) is plotted. The degree of scattering present in the evanescent field at the coverslip/sample interface was varied (A, C) while *D* was kept constant, or the degree of scattering was kept constant at 20% while varying *D* (B, D).

scattering (Figure 2D). The presence of scattered light was found to decrease the initial rate of fluorescence recovery, and to a greater extent, reduced the extent to which fluorescence recovered (Figure 2C). Nonetheless, despite a substantial degree of scattering being present in the evanescent field, fluorescence recovery was strongly sensitive to *D*, with the initial rate of recovery and extent of recovery increasing with higher *D* (Figure 2D). As described in the reversible bleaching section below, recovery from a reversibly bleached state contributes to the initial phase of recovery, and is the source of the recovery seen in the $D = 3 \times 10^{-11}$ cm^2/s simulation curve in Figure 2D.

Based on the simulations just described, both the TIR/EPI bleach depth measurements and TIR-FRAP recovery measurements are expected be sensitive to both scattering and diffusion. We included 20% scattering (see above) while estimating diffusion coefficients based on our experimental data.

TIR-FRAP measurements of fluorescent VAMP2, Syt1, and Syt-7 in chromaffin granule membranes in living cells

Primary bovine chromaffin cells were transfected with plasmids encoding secretory granule membrane proteins VAMP2-EGFP, Syt1-EGFP or msfGFP, or Syt7-EGFP, or the granule lumenal probe ss-mOxGFP (signal sequence of neuropeptide *y* fused to mOxGFP). Transfection resulted in a twofold increase in the median abundance of VAMP2 relative to nontransfected cells (Supplemental Figure S1), and a similar degree of overexpression is expected for the other transfected proteins. Four to five days after transfection, cells were transferred to a physiological salt solution (PSS), and were photobleached using high-intensity TIR excitation light to selectively photobleach fluorophores proximal to the glass interface (Figure 1). The granule membrane and lumenal proteins were photobleached for 46 and 169 ms, respectively.

For each of the proteins examined, the bleach depth (fraction of fluorescence lost) as seen by TIR and EPI illumination following a TIR bleach is displayed in scatter plots (Figure 3, A–D), and each data point represents an individual granule. For rapidly diffusing proteins (for which the bleached gradient is almost completely dissipated by the time of the probe measurement), the bleach depths as probed by either TIR or EPI illumination are expected to be equal to each other (indicated by the solid 45° black line); this was found to be the case for granules containing the granule lumenal probe ss-mOxGFP (signal sequence of neuropeptide *y* fused to mOxGFP; Figure 3D). If proteins are immobile or slowly diffusing, then the bleach depth as probed by TIR is expected to be greater relative to the bleach depth probed by EPI (because the TIR probe selectively illuminates just the region that is bleached). Indeed, this was found to be the case for granules labeled with fluorescently tagged VAMP2, Syt1, and Syt7 (Figure 3, A–C). This difference between the granule lumenal probe and membrane proteins is readily apparent when we compare the ratio of TIR/EPI bleach depths (Figure 3E), which cluster close to 1 for ss-mOxGFP, indicating equivalent bleach depths, but are greater than 1 for VAMP2, Syt1, and Syt7 (i.e., greater bleach depth evident in TIR relative to EPI). We compared Syt1 with EGFP fused to its N terminus, which is inside the granule lumen, and Syt1 with msfGFP

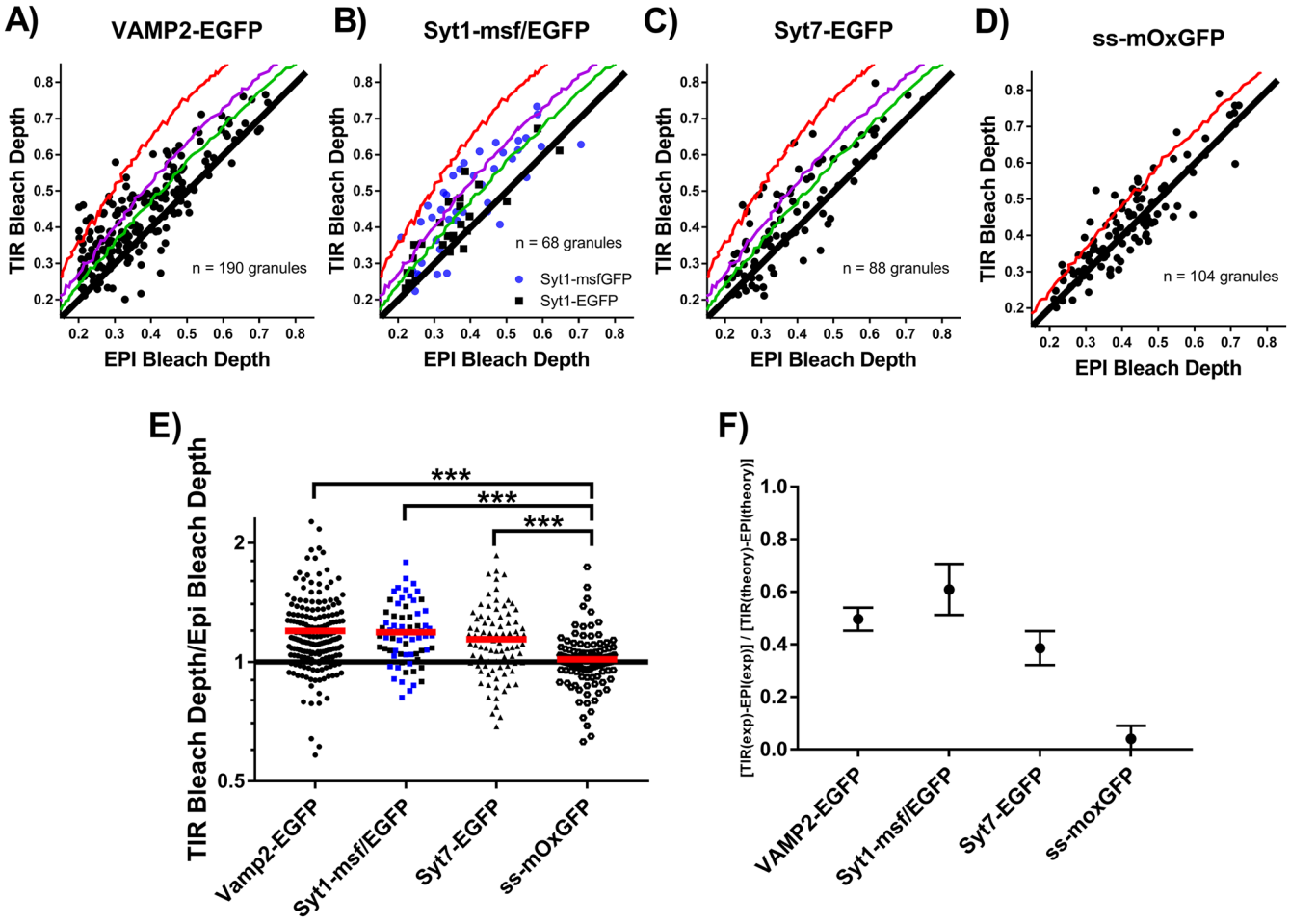

FIGURE 3: VAMP2 and synaptotagmins have low enough mobility in the granule membrane to retain a bleaching imprint within the duration of a bleaching pulse. Chromaffin cells were transfected with plasmids encoding (A) VAMP2-EGFP, (B) Syt1-msfGFP or Syt1-EGFP, (C) Syt7-EGFP, and (D) the signal sequence of NPY fused to mOxGFP (ss-mOxGFP). Chromaffin cells expressing the fusion proteins were photobleached for 46 ms (granule membrane probes), or 169 ms (ss-moxGFP) with high-intensity 488-nm excitation light in TIR mode. Fluorescence intensity was probed pre- and postbleach using low-intensity TIR and EPI illumination as described in the *Materials and Methods* section. The bleach depth (fraction of fluorescence lost) in TIR and EPI is plotted. Each data point represents an individual granule. The black 45° line is indicative of equivalent bleaching in EPI and TIR and is expected for highly mobile fluorophores. The red, purple, and green curved lines are the expected result for a fluorophore with a diffusion coefficient of $D = 3 \times 10^{-10}$ cm^2/s, photobleached in an evanescent field with 0%, 10%, or 20% scattering, respectively, and an exponential decay constant of 80 nm. The theoretical curves for membrane proteins (A–C) and for lumenal proteins (D) are somewhat different, as discussed in the *Theory* section. (E) The data shown in A–D expressed as the ratio of the bleach depths in TIR and EPI; the red line represents the median value in each group. Data from Syt1-msfGFP and Syt1-EGFP are colored blue and black, respectively. A ratio of 1 represents equivalent bleaching in TIR and EPI; *** indicates $p < 0.0001$ (unpaired Student's *t* test). (F) The ratio of experimentally observed differences in bleach depths probed with TIR and EPI illumination compared with the theoretically expected differences for an immobile fluorophore. A ratio of 0 or 1 is expected for highly mobile or immobile fluorophores, respectively. Scattering was assumed to be 0 when deriving the expected theoretical results.

fused to the C terminus, which is in the cytoplasm. We did not observe a difference between the two fusion proteins, as the TIR probed bleach depth was greater relative to the EPI probed bleach depth in both cases, indicating that the result was not sensitive to the location of the fluorophore on the protein.

Utilizing the simulations described above, we compared the experimentally observed differences in bleach depths probed with TIR and EPI illumination ("difference ratio") to the theoretically expected differences for highly mobile or immobile fluorophores (Figure 3F). A ratio of 0 or 1 is expected for highly mobile or immobile fluorophores, respectively. We found that the experimental data for ss-mOxGFP correlates closely with the expected result for highly mobile fluorophores, whereas the data from VAMP2-EGFP, Syt1-EGFP, and Syt7-EGFP granules has a ratio between 0.4 and 0.6, indicating that they are relatively immobile.

To verify that the greater fractional bleach depth evident by a TIR probe is due to photobleaching with TIR illumination, we repeated the same experiment but used high-intensity EPI illumination to photobleach fluorophores. Bleaching in EPI does not imprint a gradient of photobleached fluorophore because EPI illumination uniformly photobleaches fluorophores throughout the granule because it is not spatially selective. As expected, the bleach depth as seen by TIR and

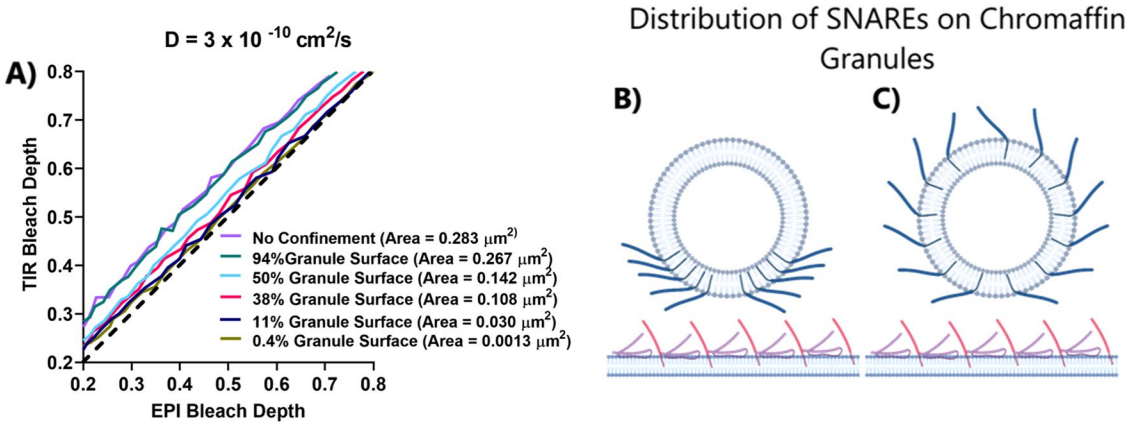

FIGURE 4: Simulations indicate that confinement of granule membrane protein reduces the difference in bleach depths measured by low-intensity TIR and EPI illumination after high-intensity TIR bleaching. Simulations were performed assuming a diffusion coefficient of 3×10^{-10} cm^2/s, 45 ms bleach time, and an evanescent decay constant of 80 nm. Molecules were either confined to defined areas at the base of a 300-nm sphere or were homogeneously distributed on the surface of the sphere. Bleach depths measured with low-intensity TIR or EPI probe illumination are plotted. The dashed line in A corresponds to equal TIR and EPI bleach depths. Confinement and homogeneous distribution of granule membrane protein are depicted in B and C, respectively. Increasing confinement decreases the difference in TIR and EPI bleach depths after high-intensity TIR bleaching.

EPI illumination following an EPI bleach is equivalent for all membrane and lumenal proteins examined (Supplemental Figure S2).

Considered together, these experiments in living chromaffin cells indicate that TIR-based photobleaching selectively imprints a gradient of fluorescence, which is long lasting and readily apparent for granules labeled with the membrane proteins VAMP2, Syt1, and Syt7 fused to EGFP, but rapidly dissipates for the granule lumenal protein ss-mOxGFP. Thus, granule membrane proteins examined are relatively immobile compared with ss-mOxGFP. (It should be noted that another granule lumen protein previously examined in this lab by the same technique, tissue plasminogen activator, is relatively immobile and sustains an imprinted gradient of fluorescence; Weiss *et al.*, 2014).

Most of the VAMP2 and Syt is not clustered at the base of chromaffin granules

In immortalized PC12 and Ins1 cells, the plasma membrane t-SNARE proteins syntaxin and SNAP25 have been shown to cluster beneath docked granules (Barg *et al.*, 2010; Knowles *et al.*, 2010; Gandasi and Barg, 2014; Yin *et al.*, 2018). The localizations of granule membrane proteins involved in exocytosis before fusion are unknown. One possibility is that VAMP2 and Syts are stably clustered at contact sites with the plasma membrane to enable docking and priming. We simulated a scenario where most of the protein is confined to such a defined area proximal to the glass interface (Figure 4). Spatial confinement has a strong influence on the bleach depths measured by TIR and EPI illumination following a TIR bleach. With strong confinement, virtually all fluorescent molecules on a granule would be at approximately the same distance from the glass interface and, therefore, be excited by the same light intensity in the exponentially decaying evanescent field. There would be no bleaching gradient. Thus, the fractional loss of intensity probed with either TIR or EPI fluorescence would be identical. In the opposite case of homogeneously distributed proteins, TIR illumination will preferentially excite the subset of those proteins that are proximal to the glass interface, the very same proteins that were preferentially exposed to the TIR bleach pulse. Consequently, the apparent bleach depth under TIR probe illumination will be deeper than that for EPI probe illumination. As our experimental data shows a clear difference between bleach depths probed by TIR and EPI illumination (Figure 3, A–C), we conclude that most of the VAMP2 and Syts are not clustered at the base of chromaffin granules.

Time dependence of recovery

Following photobleaching with high-intensity TIR excitation, we observed a time-dependent fluorescence recovery (Figure 5, A–C). The data from individual granules were grouped based on the initial bleach depth immediately after the bleach (see *Theory*). The apparent recovery was ~10% of the bleach fraction for granules expressing VAMP2-EGFP or Syt7-EGFP, and ~5% of the bleach fraction for granules expressing Syt1-EGFP or Syt1-msfGFP. As the surface of the granule is a closed system, and there is not an infinite pool of fluorophores available as in traditional TIR-FRAP experiments, recovery is expected to be less than 100%, even in the case of high mobility.

The recoveries reflect a combination of the diffusive behavior of the fluorophores and also the kinetics of reversible bleaching, wherein the fluorophore is bleached but recovers instead of being irreversibly lost (Velez and Axelrod, 1988; Sinnecker *et al.*, 2005). This issue is considered next.

Reversible bleaching

To determine the extent of reversible bleaching, EPI rather than TIR illumination was used to bleach fluorescent granule membrane proteins. Fluorescence recovery was measured with low-intensity EPI excitation (Figure 6). As EPI illumination is not spatially selective, any observed fluorescence recovery reflects purely reversible photobleaching. For the two sets of average recoveries shown, with bleach depths of 65% or 57% of the prebleach level, the reversible bleaching recovery was ~5% of the prebleach fluorescence. The half-time for recovery was ~45 ms.

To enable quantitative interpretation of the TIR bleaching experiments, and in particular to separate out the reversible bleaching recovery from the diffusive recovery contributions, we modeled three possible photochemical pathways ("modes") for reversible and irreversible bleaching, as described in the *Theory* section:

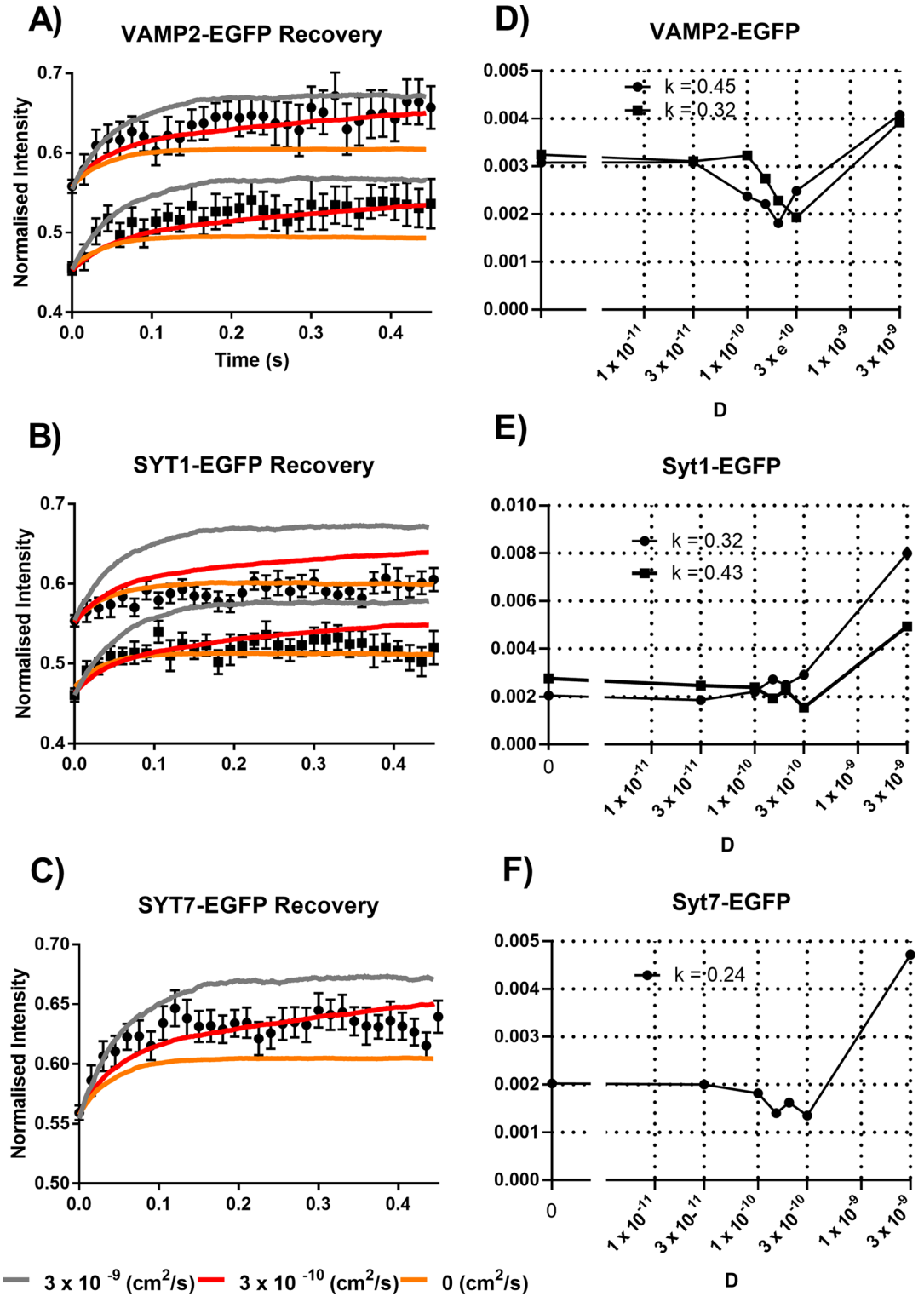

FIGURE 5: FRAP analysis of chromaffin granules expressing fluorophore-tagged membrane or lumenal proteins. Chromaffin cells expressing (A) VAMP2-EGFP, or (B) Syt1-msf or EGFP, or (C) Syt7-EGFP were photobleached with high-intensity 488 nm light in TIR mode, and fluorescence recovery was measured using low-intensity 488 nm light. Fluorescence recovery after photobleaching is shown. Experimental data were grouped into bins based on the fractional bleaching evident immediately after the photobleaching (bins: 0.4–0.5, 0.5–0.6, and each bin contains averaged data from 10 to 22 granules). Simulated theoretical curves are shown overlaid on the experimental data for three different diffusion coefficients. The kinetics and pathway (mode C) for irreversible bleaching were incorporated into the simulations. (D–F) Chi-square goodness-of-fit analysis was used to identify the simulated recovery curves that best described the experimental data. For VAMP2 (E) and Syt7 (F), the goodness of fit is better at the $D = 3 \times 10^{-10}$ (highlighted by the red horizontal line) than it is for $D = 0$ (highlighted by the orange horizontal line). The fit for Syt1 is similar for $D = 0$ and $D = 3 \times 10^{-10}$.

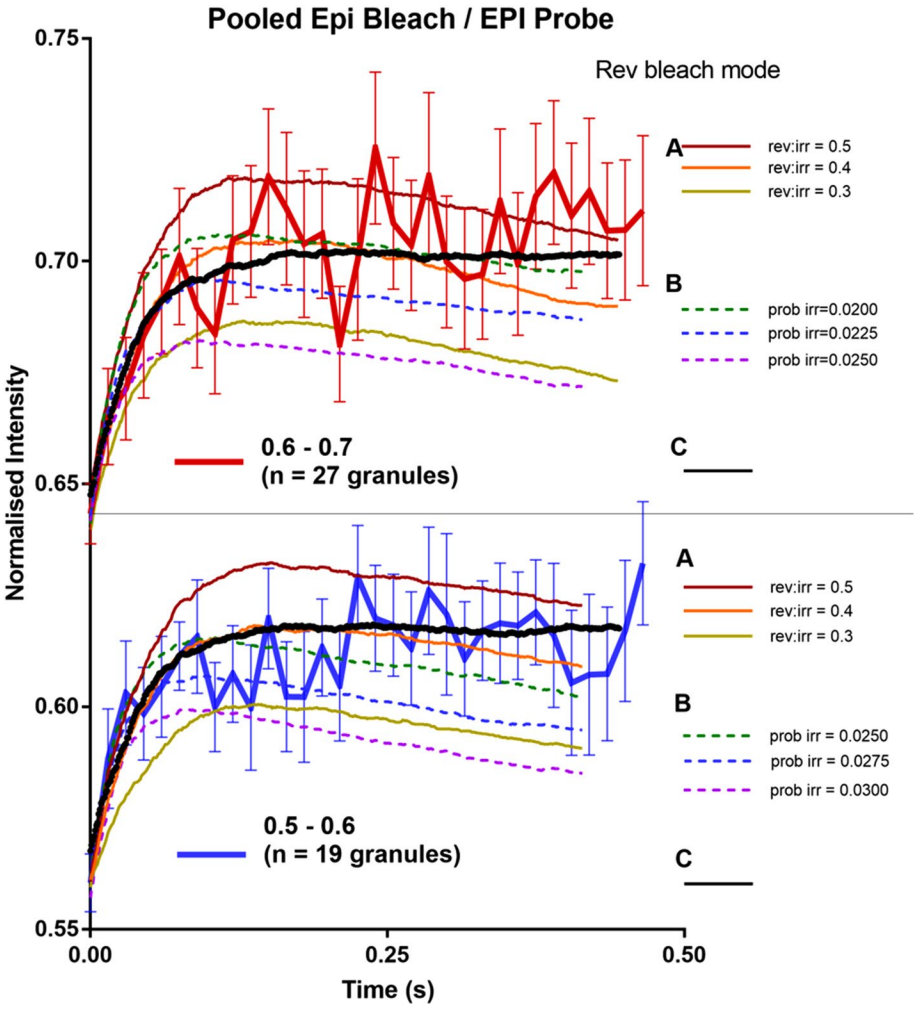

FIGURE 6: Experimental observation of fluorescence recovery of EGFP from a reversibly bleached state, and comparison with theoretical simulations, for EPI bleach and EPI probe (the case where diffusion does not matter). Chromaffin cells transfected with plasmids encoding VAMP2-EGFP, Syt1-EGFP, or Syt7-EGFP were photobleached with high-intensity 488-nm EPI excitation light. Fluorescence recovery following photobleaching was probed using low-intensity EPI illumination. The data from cells expressing the various fusion proteins were pooled based on an initial bleach depth of either 50–60% ($n = 19$ granules, blue line), or 60–70% ($n = 27$ granules, red line), and the normalized fluorescence recovery after the bleach is shown. Parameters in the simulations (shown here as smooth curves without error bars) were adjusted to produce curves that match the observed average bleach at $t = 0$ (i.e., at the end of the bleach pulse) for each of those two groups. The early recoveries reflect reversible bleaching. The incompleteness of the longer-term fluorescence reflects rapid irreversible bleaching that occurred during the bleaching pulse, and continued but more slowly during the probe phase. Three theoretically possible modes of reversible recovery were simulated, with a range of the most relevant adjustable parameter for each, as follows: (Mode A, solid colored lines) Reversible and irreversible bleaching can occur from an unbleached ground state, each with its own probability; the ratio of these probabilities (indicated as "rev:irr") strongly affects the match of simulations to experimental data. (Mode B, dashed colored lines) Irreversible bleaching can spontaneously occur from a reversibly bleached state without the need for the fluorophore to encounter a second photon. The probability (in each time increment) for this second step to occur is indicated as "prob irr." (Mode C, solid black line) Irreversible bleaching can only occur from an already-reversibly bleached state and the irreversible bleaching step requires another photon. Parameters for the irreversible part of the bleach were chosen to best match the experimental data and "rev:irr" was set to 0.15. These same parameters were then used in all the simulations involving TIR and diffusion. The characteristic time parameters for reversible recovery were chosen to be 45 ms for modes A and C and 75 ms for mode B. For all modes, the intensity of the bleach pulse was adjusted so that the simulation curve matched the experimental data at $t = 0$.

1) irreversible and reversible photobleaching occur in parallel. Any single fluorophore may undergo either one or the other of those processes; 2) irreversible photobleaching can only occur from the reversibly bleached state at a random time, independent of light intensity; or 3) irreversible photobleaching can only occur from the reversibly bleached state, but only if a second photon is absorbed. In the third situation, a fluorophore has to encounter a minimum of two photons to be irreversibly photobleached: one to induce reversible photobleaching, and the second to cause irreversible photobleaching. Experimentally, we found that only the third mode 3) adequately described the data (Figure 6) obtained for EPI bleach/EPI probe. In the first two modes (A and B) of reversible recovery, there is initial fluorescence recovery followed by gradual fading due to irreversible photobleaching caused by low-intensity probe illumination. No combination of parameter probability rates in those two modes can produce recovery curves that match the experimental observations, which do not show much fluorescence fading during the probe phase. However, the third mode 3) does not produce as much fading during the probe phase; only the probability parameters of mode C can be adjusted to closely match the experimental data.

There is a reason why modes A and B unavoidably exhibit fading during the probe phase, whereas mode C does not. The ratio of probe-to-bleach intensities is fixed in the experiments at 1:100. But the probe phase has a duration of 10 times that of the bleach pulse. Because irreversible bleaching in both modes A and B depend linearly on intensity, one would then expect the total bleaching to be fully 1/10 that of what occurs during the bleach pulse. That accounts for the probe phase fading. In contrast, irreversible bleaching in mode C is a two-photon process. It depends on the square of the probe-to-bleach intensity ratio (i.e., 1:10,000), thereby leading to much less bleaching during the probe phase, and is more in line with what is actually observed.

Estimation of diffusion coefficients of granule membrane proteins

To determine diffusion coefficients, we generated a series of simulated TIR-FRAP recovery curves based upon diffusion on the surface of a sphere of the same diameter as a chromaffin granule (300 nm). Diffusion coefficients were varied and the results compared with the experimental TIR-fluorescence

recovery data. The reversible bleaching probability and kinetics parameters determined for the best fit in on EPI bleach/EPI probe data (i.e., mode C as described in the subsection above) were incorporated into the simulations. Scattering was assumed to account for 20% of the total bleaching intensity at the glass interface (see above). A diffusion coefficient of 0 represents recovery observed solely from a reversibly bleached state. We used chi-square-based goodness-of-fit analysis to determine the best fit (i.e., the diffusion coefficient that best described the data) in an unbiased way. The initial rising phase of recovery from VAMP2-EGFP and Syt7-EGFP expressing granules was best described by diffusion coefficients of 1.5 to 3×10^{-10} cm^2/s (Figure 5, D and F). A diffusion coefficient of 3×10^{-9} cm^2/s or greater results in a suboptimal fit. Syt1-EGFP data could not be distinguished from a diffusion coefficient of 0 (Figure 5E), indicating that recovery observed from Syt1-EGFP expressing granules was likely only from a reversibly bleached state. Reversible bleaching limits the ability to estimate very low diffusion coefficients.

DISCUSSION

The granule membrane proteins VAMP2 (a v-SNARE) and Syt 1 and Syt 7 (Ca^{2+} sensors) are proposed to interact with lipids and cognate SNAREs on the plasma membrane to enable regulated exocytosis. The molecular organization of VAMP2 and Syts on secretory granules and their diffusion characteristics, thus, likely influence successful interactions with plasma membrane proteins. In this study we measured the mobility VAMP2, Syt1, and Syt7 in the membrane of chromaffin granules in living cells using a TIRF-based technique that is not limited by the axial resolution of the microscope. We found that VAMP2-EGFP and Syt7-EGFP have a finite mobility with $D = (1.5–3) \times 10^{-10}$ cm^2/s and Syt1-EGFP has a mobility that is somewhat lower, here undetectably different from 0. Furthermore, the bleaching characteristics of all three proteins are consistent with their being distributed over the granule membrane surface. We consider the implications of these findings on regulated exocytosis in the following.

Diffusion of VAMP2, Syt-1, and Syt-7 on chromaffin granule and plasma membranes

The in situ mobility of membrane proteins varies by almost two orders of magnitude depending upon the subcellular localization (Lippincott-Schwartz *et al.*, 1998; Nehls *et al.*, 2000; Ramadurai *et al.*, 2009; Kreutzberger *et al.*, 2019). Golgi proteins have diffusion constants of ~5×10^{-9} cm^2/s, whereas plasma membrane proteins generally have the lowest mobilities with diffusion coefficients, ~10^{-10} cm^2/s. Indeed, the plasma membrane SNARE protein syntaxin has mobilities ranging from 3.9×10^{-10} to 2×10^{-11} cm^2/s (Gandasi and Barg, 2014). The relatively lower mobilities of plasma membrane proteins reflect interaction with intracellular cytoskeletal proteins and extracellular matrix proteins (Jacobson *et al.*, 1987; Runions *et al.*, 2006; Ramadurai *et al.*, 2010; Alenghat and Golan, 2013; Trimble and Grinstein, 2015). Transfected VAMP2 and Syt1 disperse into the plasma membrane upon fusion, allowing the estimation of apparent diffusion constants (in the plasma membrane). VAMP-2-GFP diffuses from the site of exocytosis in the plasma membrane with an apparent diffusion constant of 2×10^{-9} cm^2/s (Allersma *et al.*, 2004). Transfected Syt1-pHluorin diffuses into the plasma membrane much more slowly, with an apparent diffusion constant of 6×10^{-11} cm^2/s (Rao *et al.*, 2014), similar to some endogenous plasma membrane proteins. The slower diffusion of Syt1 in the plasma membrane may also reflect the slow rate of dissociation of the protein from the fused granule membrane as well as interaction with intracellular and extracellular components. Syt7 barely disperses upon fusion, possibly because a stable, narrow fusion pore restricts dispersion into the plasma membrane (Rao *et al.*, 2014).

The diffusion coefficient of VAMP2 in the chromaffin granule membrane, $(1.5–3) \times 10^{-10}$ cm^2/s, was an order of magnitude slower than its postfusion diffusion in the plasma membrane (Allersma *et al.*, 2004). Syt7 had a mobility comparable to VAMP2 on the chromaffin granule membrane, and faster than its postfusion diffusion in the plasma membrane. Syt1 diffusion in the granule membrane was too slow to be detected, suggesting a slower granule membrane diffusion compared with VAMP2 and Syt7.

Assembly of multiple fusion complexes

There is general agreement that fusion requires the formation of multiple *trans*-SNARE complexes at the fusion site. For example, reconstitution-based biochemical analyses have suggested that as little as three SNARE complexes are sufficient to form a fusion pore (Karatekin *et al.*, 2010; Shi *et al.*, 2012; Bao *et al.*, 2018). In hippocampal synapses, two copies of VAMP2 may be sufficient for synaptic vesicle fusion and it was suggested that diffusion of a VAMP2 molecule was necessary to consummate the fusion reaction (Sinha *et al.*, 2011). A study in isolated chromaffin cells found that at least three SNARE complexes are required for efficient exocytosis (Mohrmann *et al.*, 2010). Synaptotagmin is also required for Ca^{2+}-triggered fusion. Although there is disagreement whether synaptotagmin interacts with SNAREs (Dai *et al.*, 2007; Brewer *et al.*, 2015; Park *et al.*, 2015; Zhou *et al.*, 2015), there is strong evidence of functional cooperation between Syt1 and VAMP2 (Bhalla *et al.*, 2006; Wang *et al.*, 2016; Das *et al.*, 2020). It is plausible that there are an equal number of Syt1 and SNARE complexes at the fusion site.

The assembly of the necessary number of fusion complexes depends upon the local availability of the component proteins. Assuming an initial homogeneous distribution of protein, we calculated the minimum time required for four copies of VAMP2 and Syt 7 to reach an area encompassed by an early fusion pore of 1 nm radius. (We speculated that four copies would be sufficient to enable both fusion pore opening and subsequent expansion.) To estimate the time required, we modeled the granule membrane as an infinite plane containing VAMP2 and Syt 7 and modeled the fusion pore as a "perfect sink" that instantly and permanently traps molecules that it encounters (Eq. 5.79 in Crank, 1979). Because this method does not take into account the depletion of the finite pool of molecules in the granule membrane, it estimates the *minimum* time required. Because the copy numbers of VAMP2 and Syt on large dense core secretory granules are unknown, we investigated a range of protein densities based upon the protein densities in synaptic vesicles (Takamori *et al.*, 2006) of 820–26,000 copies/μm^2 (corresponds to 5–160 copies/synaptic vesicle). As expected, diffusion times decreased as protein abundance increased (Figure 7A) with times ranging from 200 ms for the lowest protein density to 2 ms for the highest. If the densities of VAMP2 and synaptotagmin in chromaffin granules were the same as in synaptic vesicles (70 and 15 copies of VAMP2 and synaptotagmin, respectively, in synaptic vesicles), the time required for four copies to be captured by a 1-nm radius pore complex would be greater than 7 and 50 ms, respectively (Figure 7A). As the capture radius increases, the capture time decreases (Figure 7B).

Possible influence of VAMP2 and Syt diffusion on *trans*-SNARE formation, granule docking, and fusion

An unknown factor in considering whether VAMP2 and Syt diffusion influences rates of exocytosis is the latency between *trans*-SNARE

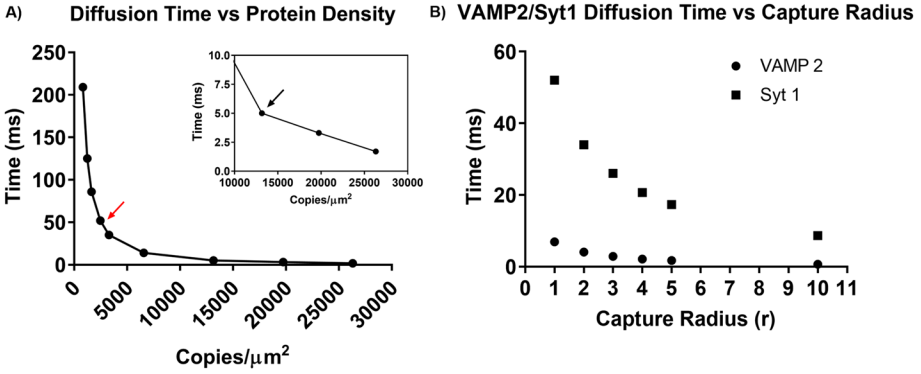

FIGURE 7: Influence of diffusion and protein abundance on the time required for proteins to reach a fusion pore of a defined radius. (A) The influence of vesicle membrane protein abundance on the time required for proteins to reach a fusion pore. Given a D of 3×10^{-10} cm^2/s, we calculated the amount of time needed for four copies of a protein to reach a fusion pore 1 nm in radius, with protein density ranging from 820 to 26,000 copies/μm^2. The inset shows a magnified view of the 12,000–26,000 copies/μm^2 range. The red and black arrows show Syt1 and VAMP2 densities on synaptic vesicles, respectively. (B) Time required for four copies of Syt1 or VAMP2 to arrive at a fusion pore of a defined radius. A diffusion coefficient of 3×10^{-10} cm^2/s was used to describe the mobility of both VAMP2 and Syt7, and the concentration of VAMP2 and Syt7 was set to the same densities as on synaptic vesicles (equivalent to 70 copies of VAMP2 and 15 copies of Syt per synaptic vesicle). The diffusion time calculations were performed as described in the *Discussion* section.

complex formation and subsequent fusion. There are at least two possibilities. As SNARE and Syt proteins play a role in docking, stable *trans*-SNARE complexes have been postulated to form before fusion, and await the Ca^{2+} trigger for secretion (Wu *et al.*, 2012; Imig *et al.*, 2014). In this case, the mobilities of VAMP2 and Syt 1 or Syt 7 may be low enough to limit the rate of formation of complexes but not the subsequent rate of fusion pore formation. Apposition of granules to the plasma membrane induces within seconds the formation of a syntaxin cluster on the adjacent plasma membrane (Barg *et al.*, 2010; Knowles *et al.*, 2010; Gandasi and Barg, 2014) and it is tempting to envision that the cluster reflects the formation of *trans*-SNARE complexes with VAMP2 in the granule membrane. This is probably not the case. The initial syntaxin cluster contains little SNAP25 (Gandasi and Barg, 2014) and does not require functional VAMP2 on the granule membrane (Barg *et al.*, 2010). Clusters are unstable and fluctuate in the same spot with lifetimes of 1–2 s (Barg *et al.*, 2010). Syntaxin cluster formation more likely reflects a docking step that precedes fusion (Gandasi and Barg, 2014; Yin *et al.*, 2018). Stable, *trans*-SNARE complexes, if they occur, probably form subsequent to syntaxin clustering and docking.

A second possibility is that the interaction of the v- and t-SNARES is all or none and very rapid, without prior *trans*-SNARE engagement (Jahn and Fasshauer, 2012). Rapid and complete interaction is driven by the large downhill energy gradient for SNARE complex formation. Indeed, förster resonance energy transfer (FRET) measurements suggest that the plasma membrane t-SNARE acceptor complex of syntaxin and SNAP25 for granule VAMP2 forms only shortly (100 ms) before fusion (Wang *et al.*, 2008; Zhao *et al.*, 2013; Holz and Bittner, 2020). Additionally, granules continue to jitter as much as 100 nm (much greater than the ~10-nm length of the tetrahelical SNARE complex) within 100 ms of fusion (Allersma *et al.*, 2006; Degtyar *et al.*, 2007). Both these observations argue against the formation of *trans*-SNARE complexes hundreds of milliseconds or longer before fusion. If this pathway is correct, then formation of the initial fusion pore could be limited by the diffusion times to the fusion site of VAMP2 and/or synaptotagmin (at least 7 and 50 ms, respectively, at protein densities estimated for synaptic vesicles and slower for lower protein densities). Stochastic variation in protein abundance on individual vesicles would likely result in variable diffusion times to a nascent fusion pore.

We should note that the greater bleach depth measured by TIR than EPI illumination in our TIR-FRAP experiments indicates that a significant fraction of the transfected VAMP2 and Syt molecules are not normally clustered at the granule-plasma membrane interface. This is consistent with recent superresolution/EM imaging that indicates that Rab proteins and effectors are randomly distributed on the secretory granule membrane in PC12 cells (Prasai *et al.*, 2021).

How do diffusion times compare to the actual kinetics of fusion in response to a stimulus? Following sudden elevation of intracellular Ca^{2+} in rat chromaffin cells, there is a burst of fusion events whose kinetics are fit by double exponentials (Chow *et al.*, 1992; Heinemann *et al.*, 1994; Voets, 2000) with time constants of ~1 s and 100 ms at 10 μM Ca^{2+} (Voets, 2000; Voets *et al.*, 2001). Fusion does not begin immediately, but with delays of ~10 and ~200 ms for the fast and slow components, respectively. The delays for either component and the fusion rate of the fast component are comparable to the estimated diffusion times for four copies to be captured by a 1-nm radius pore complex. It is, therefore, possible if the formation of *trans*-SNARE complexes drives fusion, that diffusion to the fusion site of VAMP2 and/or Syt could influence fusion kinetics.

With either pathway, preformed *trans*-SNARE complexes or *trans*-SNARE complexes immediately driving fusion, protein diffusion may play another role in exocytosis. Both fusion pore stability and the subsequent rate of fusion pore expansion in reconstituted fusion reactions increase with increasing numbers of SNARE complexes (Wu *et al.*, 2017; Bao *et al.*, 2018). Diffusion of VAMP2 and synaptotagmin into the nascent fusion pore may, therefore, influence both its stability and expansion.

In summary, we have exploited the submicroscopic resolution of TIRF microscopy to estimate the mobility of granule membrane proteins important in exocytosis in living cells. To our knowledge, these are the first such measurements. The finite mobility of VAMP2 and Syt 7 suggests that these proteins do not have to be initially present at the nascent fusion site when the granule interacts with the plasma membrane. Instead, their subsequent diffusion to the site could enable formation of *trans*-SNARE complexes. Calculations based on their measured mobilities and the lack of significant confinement of the proteins on individual secretory granules raise the possibility that their diffusion could be a factor that influences the rates of fast processes in exocytosis that rely on multiple protein copies.

MATERIALS AND METHODS

Request a protocol through *Bio-protocol*.

Chromaffin cell culture and transfection

Bovine chromaffin cells were isolated and transfected using the Neon Transfection System (Thermo Fisher Scientific) as previously described (Bohannon *et al.*, 2017; Abbineni *et al.*, 2018). For transfection of GFP-tagged granule membrane proteins, 1 μg of the

plasmid encoding the fusion protein was used per 10^6 cells. All plasmids used were verified by DNA sequencing, and details regarding the promoter and linker sequences are provided in the Supplement (Supplemental Table S1). Imaging experiments were performed in PSS containing 145 mM NaCl, 5.6 mM KCl, 2.2 mM $CaCl_2$, 0.5 mM $MgCl_2$, 5.6 mM glucose, and 15 HEPES, pH 7.4. All live-cell imaging experiments were performed at 34°C 4–6 d after cell isolation.

TIR-FRAP microscopy and image analysis

Prismless (through-the-objective) TIR excitation was obtained by directing a laser beam from a 100-mW solid-state (488-nm) laser (Coherent OBIS, CA) onto a computer-controlled galvanometer mirror and then toward a side port of an Olympus inverted microscope. The aligned excitation beam was focused and positioned near the periphery of the back focal plane of a 60× 1.49-NA, oil immersion objective (Olympus) so that the laser beam was incident on the coverslip at ~70° from the normal giving a decay constant for the evanescent field of ~80 nm. The galvanometer mirrors were computer controlled though a DAQ board (National Instruments) and a custom LabView program, and allowed for rapid switching between TIR and EPI excitation by modulation of the incidence angle. To allow for rapid switching between high-intensity bleach and low-intensity probe excitation, the OBIS laser was operated in analogue modulation mode and the input voltage was controlled by the same custom LabView program that controlled the galvanometer mirrors. Fluorescence emission was collected through the 1.49-NA objective, and images were acquired using a CMOS camera (Prime, Photometrics).

Two different but related types of TIR/EPI data were gathered: "bleach depth" and "FRAP." Depending on the experiment, the bleach or the probe could be set as either TIR or EPI. For TIR/EPI bleach depth measurements, single sets of EPI and TIR images were utilized, one set immediately before and one set immediately after the bleach pulse, which lasted 46 ms (as shown in Figure 1B). For TIR and EPI-FRAP measurements, a time sequence of numerous TIR or EPI images was utilized both before and after the bleach pulse. For both types of measurements, images were acquired at a rate of 65 Hz. The images were subsequently processed using ImageJ (Fiji distribution) and data analysis was performed using custom programs written in Python and IDL, the central program "diffusionshellsim" is provided in the Supplement, and all custom programs used will be provided upon request. Granules harboring GFP-tagged proteins were identified as bright puncta and changes in fluorescence intensities were monitored over time within a defined circular region of interest (ROI) that encompassed the whole puncta. Background intensity was measured from a circular region immediately adjacent to the granule, and subtracted from the granule fluorescence intensity. Only granules with ROI average intensity at least 15 % greater than background intensity throughout the movie (i.e., before and after photobleaching) were included in the final analysis. In the TIR and EPI bleach depth experiments, the emission intensities from individual granules were averaged over a set of three successive frames to reduce shot noise. For the TIR and EPI-FRAP experiments, emission intensities were used without any averaging. All recovery curves presented are averages of fluorescence recovery observed from several granules (n = number of granules, and is noted in figure legends), and error bars represent standard errors of the mean. Statistical and computational analysis of fluorescence recovery is described in the *Theory* and *Results* sections.

ACKNOWLEDGMENTS

We thank Kevin P. Bohannon and Mary A. Bittner for many helpful discussions. msfGFP used to construct the C-terminal syt1-msfGFP fusion protein was a gift from Benjamin Glick (University of Chicago). This work was supported by National Institutes of Health (NIH) Grant no. R01-170553 to R.W.H. and D.A. E.R.C. is an Investigator of the Howard Hughes Medical Institute, and acknowledges support from NIH Grants no. MH061876 and no. NS097362.

REFERENCES

Abbineni PS, Bittner MA, Axelrod D, Holz RW (2018). Chromogranin A, the major lumenal protein in chromaffin granules, controls fusion pore expansion. J Gen Physiol 151, 118–130.

Alenghat FJ, Golan DE (2013). Membrane protein dynamics and functional implications in mammalian cells. Curr Top Membr 72, 89–120.

Allersma MW, Bittner MA, Axelrod D, Holz RW (2006). Motion matters: secretory granule motion adjacent to the plasma membrane and exocytosis. Mol Biol Cell 17, 2424–2438.

Allersma MW, Wang L, Axelrod D, Holz RW (2004). Visualization of regulated exocytosis with a granule-membrane probe using total internal reflection microscopy. Mol Biol Cell 15, 4658–4668.

Axelrod JJ, Axelrod D (2021). Light scattering in TIRF microscopy: a theoretical study of the limits to surface selectivity. Biophys J 120, 2952–2968.

Bao H, Das D, Courtney NA, Jiang Y, Briguglio JS, Lou X, Roston D, Cui Q, Chanda B, Chapman ER (2018). Dynamics and number of trans-SNARE complexes determine nascent fusion pore properties. Nature 554, 260–263.

Barg S, Knowles MK, Chen X, Midorikawa M, Almers W (2010). Syntaxin clusters assemble reversibly at sites of secretory granules in live cells. Proc Natl Acad Sci USA 107, 20804–20809.

Bhalla A, Chicka MC, Tucker WC, Chapman ER (2006). Ca^{2+}-synaptotagmin directly regulates t-SNARE function during reconstituted membrane fusion. Nat Struct Mol Biol 13, 323–330.

Bohannon KP, Bittner MA, Lawrence DA, Axelrod D, Holz RW (2017). Slow fusion pore expansion creates a unique reaction chamber for co-packaged cargo. J Gen Physiol 149, 921–934.

Brewer KD, Bacaj T, Cavalli A, Camilloni C, Swarbrick JD, Liu J, Zhou A, Zhou P, Barlow N, Xu J, *et al*. (2015). Dynamic binding mode of a Synaptotagmin-1-SNARE complex in solution. Nat Struct Mol Biol 22, 555–564.

Brunstein M, Herault K, Oheim M (2014a). Eliminating unwanted far-field excitation in objective-type TIRF. Part II. Combined evanescent-wave excitation and supercritical-angle fluorescence detection improves optical sectioning. Biophys J 106, 1044–1056.

Brunstein M, Teremetz M, Herault K, Tourain C, Oheim M (2014b). Eliminating unwanted far-field excitation in objective-type TIRF. Part I. Identifying sources of nonevanescent excitation light. Biophys J 106, 1020–1032.

Chow RH, von Ruden L, Neher E (1992). Delay in vesicle fusion revealed by electrochemical monitoring of single secretory events in adrenal chromaffin cells. Nature 356, 60–63.

Crank J (1979). The Mathematics of Diffusion, Oxford, UK: Oxford University Press.

Dai H, Shen N, Arac D, Rizo J (2007). A quaternary SNARE-synaptotagmin-Ca^{2+}-phospholipid complex in neurotransmitter release. J Mol Biol 367, 848–863.

Das D, Bao H, Courtney KC, Wu L, Chapman ER (2020). Resolving kinetic intermediates during the regulated assembly and disassembly of fusion pores. Nat Commun 11, 231.

Degtyar VE, Allersma MW, Axelrod D, Holz RW (2007). Increased motion and travel, rather than stable docking, characterize the last moments before secretory granule fusion. Proc Natl Acad Sci USA 104, 15929–15934.

Gandasi NR, Barg S (2014). Contact-induced clustering of syntaxin and munc18 docks secretory granules at the exocytosis site. Nat Commun 5, 3914.

Heinemann C, Chow RH, Neher E, Zucker RS (1994). Kinetics of the secretory response in bovine chromaffin cells following flash photolysis of caged Ca^{2+}. Biophys J 67, 2546–2557.

Holz RW, Bittner MA (2020). Roles for the SNAP25 linker domain in the fusion pore and a dynamic plasma membrane SNARE "acceptor" complex. J Gen Physiol 152, e202012619.

Imig C, Min SW, Krinner S, Arancillo M, Rosenmund C, Sudhof TC, Rhee J, Brose N, Cooper BH (2014). The morphological and molecular nature of synaptic vesicle priming at presynaptic active zones. Neuron 84, 416–431.

Jacobson K, Ishihara A, Inman R (1987). Lateral diffusion of proteins in membranes. Annu Rev Physiol 49, 163–175.

Jahn R, Fasshauer D (2012). Molecular machines governing exocytosis of synaptic vesicles. Nature 490, 201–207.
Karatekin E, Di Giovanni J, Iborra C, Coleman J, O'Shaughnessy B, Seagar M, Rothman JE (2010). A fast, single-vesicle fusion assay mimics physiological SNARE requirements. Proc Natl Acad Sci USA 107, 3517–3521.
Karatekin E, Tran VS, Huet S, Fanget I, Cribier S, Henry JP (2008). A 20-nm step toward the cell membrane preceding exocytosis may correspond to docking of tethered granules. Biophys J 94, 2891–2905.
Knowles MK, Barg S, Wan L, Midorikawa M, Chen X, Almers W (2010). Single secretory granules of live cells recruit syntaxin-1 and synaptosomal associated protein 25 (SNAP-25) in large copy numbers. Proc Natl Acad Sci USA 107, 20810–20815.
Kreutzberger AJB, Ji M, Aaron J, Mihaljevic L, Urban S (2019). Rhomboid distorts lipids to break the viscosity-imposed speed limit of membrane diffusion. Science 363, aao0076.
Lippincott-Schwartz J, Cole N, Presley J (1998). Unravelling Golgi membrane traffic with green fluorescent protein chimeras. Trends Cell Biol 8, 16–20.
Mattheyses AL, Axelrod D (2006). Direct measurement of the evanescent field profile produced by objective-based total internal reflection fluorescence. J Biomed Opt 11, 014006.
Mohrmann R, de Wit H, Verhage M, Neher E, Sorensen JB (2010). Fast vesicle fusion in living cells requires at least three SNARE complexes. Science 330, 502–505.
Nehls S, Snapp EL, Cole NB, Zaal KJ, Kenworthy AK, Roberts TH, Ellenberg J, Presley JF, Siggia E, Lippincott-Schwartz J (2000). Dynamics and retention of misfolded proteins in native ER membranes. Nat Cell Biol 2, 288–295.
Nofal S, Becherer U, Hof D, Matti U, Rettig J (2007). Primed vesicles can be distinguished from docked vesicles by analyzing their mobility. J Neurosci 27, 1386–1395.
Park Y, Seo JB, Fraind A, Perez-Lara A, Yavuz H, Han K, Jung SR, Kattan I, Walla PJ, Choi M, *et al*. (2015). Synaptotagmin-1 binds to PIP(2)-containing membrane but not to SNAREs at physiological ionic strength. Nat Struct Mol Biol 22, 815–823.
Plattner H, Artalejo AR, Neher E (1997). Ultrastructural organization of bovine chromaffin cell cortex-analysis by cryofixation and morphometry of aspects pertinent to exocytosis. J Cell Biol 139, 1709–1717.
Prasai B, Haber GJ, Strub MP, Ahn R, Ciemniecki JA, Sochacki KA, Taraska JW (2021). The nanoscale molecular morphology of docked exocytic dense-core vesicles in neuroendocrine cells. Nat Commun 12, 3970.
Ramadurai S, Duurkens R, Krasnikov VV, Poolman B (2010). Lateral diffusion of membrane proteins: consequences of hydrophobic mismatch and lipid composition. Biophys J 99, 1482–1489.
Ramadurai S, Holt A, Krasnikov V, van den Bogaart G, Killian JA, Poolman B (2009). Lateral diffusion of membrane proteins. J Am Chem Soc 131, 12650–12656.
Rao TC, Passmore DR, Peleman AR, Das M, Chapman ER, Anantharam A (2014). Distinct fusion properties of synaptotagmin-1 and synaptotagmin-7 bearing dense core granules. Mol Biol Cell 25, 2416–2427.
Rizo J, Südhof TC (2012). The membrane fusion enigma: SNAREs, SM Proteins, and their accomplices-guilty as charged? Annu Rev Cell Dev Biol 28, 279–308.
Runions J, Brach T, Kuhner S, Hawes C (2006). Photoactivation of GFP reveals protein dynamics within the endoplasmic reticulum membrane. J Exp Bot 57, 43–50.
Shi L, Shen QT, Kiel A, Wang J, Wang HW, Melia TJ, Rothman JE, Pincet F (2012). SNARE proteins: one to fuse and three to keep the nascent fusion pore open. Sci. Signal. 335, 1355.
Sinha R, Ahmed S, Jahn R, Klingauf J (2011). Two synaptobrevin molecules are sufficient for vesicle fusion in central nervous system synapses. Proc Natl Acad Sci USA 108, 14318–14323.
Sinnecker D, Voigt P, Hellwig N, Schaefer M (2005). Reversible photobleaching of enhanced green fluorescent proteins. Biochem 44, 7085–7094.
Sudhof TC (2013). Neurotransmitter release: the last millisecond in the life of a synaptic vesicle. Neuron 80, 675–690.
Takamori S, Holt M, Stenius K, Lemke EA, Gronborg M, Riedel D, Urlaub H, Schenck S, Brugger B, Ringler P, *et al*. (2006). Molecular anatomy of a trafficking organelle. Cell 127, 831–846.
Thompson NL, Burghardt TP, Axelrod D (1981). Measuring surface dynamics of biomolecules by total internal reflection fluorescence with photobleaching recovery or correlation spectroscopy. Biophys J 33, 435–454.
Trimble WS, Grinstein S (2015). Barriers to the free diffusion of proteins and lipids in the plasma membrane. J Cell Biol 208, 259–271.
Velez M, Axelrod D (1988). Polarized fluorescence photobleaching recovery for measuring rotational diffusion in solutions and membranes. Biophys J 53, 575–591.
Voets T (2000). Dissection of three Ca^{2+}-dependent steps leading to secretion in chromaffin cells from mouse adrenal slices. Neuron 28, 537–545.
Voets T, Moser T, Lund PE, Chow RH, Geppert M, Sudhof TC, Neher E (2001). Intracellular calcium dependence of large dense-core vesicle exocytosis in the absence of synaptotagmin I. Proc Natl Acad Sci USA 98, 11680–11685.
Wang L, Bittner MA, Axelrod D, Holz RW (2008). The structural and functional implications of linked SNARE motifs in SNAP25. Mol Biol Cell 19, 3944–3955.
Wang S, Li Y, Ma C (2016). Synaptotagmin-1 C2B domain interacts simultaneously with SNAREs and membranes to promote membrane fusion. eLife 5, e14211.
Weiss AN, Bittner MA, Holz RW, Axelrod D (2014). Protein mobility within secretory granules. Biophys J 107, 16–25.
Wu Z, Bello OD, Thiyagarajan S, Auclair SM, Vennekate W, Krishnakumar SS, O'Shaughnessy B, Karatekin E (2017). Dilation of fusion pores by crowding of SNARE proteins. eLife 6, e22964.
Wu Y, Gu Y, Morphew MK, Yao J, Yeh FL, Dong M, Chapman ER (2012). All three components of the neuronal SNARE complex contribute to secretory vesicle docking. J Cell Biol 198, 323–330.
Yin P, Gandasi NR, Arora S, Omar-Hmeadi M, Saras J, Barg S (2018). Syntaxin clusters at secretory granules in a munc18-bound conformation. Mol Biol Cell 29, 2700–2708.
Zhao Y, Fang Q, Herbst AD, Berberian KN, Almers W, Lindau M (2013). Rapid structural change in synaptosomal-associated protein 25 (SNAP25) precedes the fusion of single vesicles with the plasma membrane in live chromaffin cells. Proc Natl Acad Sci USA 110, 14249–14254.
Zhou Q, Lai Y, Bacaj T, Zhao M, Lyubimov AY, Uervirojnangkoorn M, Zeldin OB, Brewster AS, Sauter NK, Cohen AE, *et al*. (2015). Architecture of the synaptotagmin-SNARE machinery for neuronal exocytosis. Nature 525, 62–67.